Shear-Enhanced Crystallization in Isotactic Polypropylene. In-Situ Synchrotron SAXS and WAXD

Guruswamy Kumaraswamy,[§] Ravi K. Verma,[†] Julia A. Kornfield,*[,†] Fengji Yeh,[‡] and Benjamin S. Hsiao[‡]

Division of Chemistry and Chemical Engineering, California Institute of Technology, Pasadena, California 91125, and Chemistry Department, State University of New York, Stony Brook, Stony Brook, New York 11794

Received December 4, 2003; Revised Manuscript Received August 11, 2004

ABSTRACT: In-situ synchtrotron small-angle X-ray scattering (SAXS) and wide-angle X-ray diffraction (WAXD) are used to follow the isothermal crystallization (lamellar thickness, crystallinity, orientation, and parent-to-daughter ratio) of a polydisperse isotactic polypropylene subjected to "short term shearing" as a function of imposed shear stress, shearing duration, and crystallization temperature. The X-ray data are interpreted in view of the real-space morphological information from ex-situ microscopy. Under "mild" shearing conditions (shear stress less than a critical value and shearing duration less than a critical time), needlelike nuclei are induced during shear but are so far apart that crystallites splay substantially as they grow to form somewhat distorted spherulites; the X-ray results show weakly oriented growth on a time scale that is rapid compared to quiescent crystallization and show that the orientation distribution broadens as crystallization progresses. Stronger shearing leads to the elaboration of these nuclei into threadlike structures that template the formation of highly oriented crystals with fiberlike orientation. The parent-to-daughter ratio is influenced by both temperature and flow. As expected, increasing the crystallization temperature leads to fewer daughter crystals relative to the parents. Shear also enhances the formation of parents relative to daughters: as parent crystals form with their chain axis along the flow direction, the epitaxial daughter crystals have their chain axis in an unfavorable direction, perpendicular to the flow.

1. Introduction and Background

The engineering performance of a product made from a semicrystalline polymer is determined by the degree of crystallinity and by the arrangement of crystallites[1] from the unit cell (angstrom scale) to the lamellar (nanoscale) and gross macroscopic level (micron scale). Therefore, over the past few decades researchers have sought an understanding of the manner in which crystalline microstructure develops over this entire hierarchy of length scales. However, the complexity of polymer crystallization, especially when it is influenced by flow, has frustrated their efforts, and the molecular underpinnings of the flow-phase transition coupling are understood only at a phenomenological level. Recently,[2−5] we have been investigating shear-enhanced crystallization of a particular polydisperse isotactic polypropylene that is representative of commercial Ziegler−Natta iPP in its distribution of tacticity and molar mass (PP-300/6) under well-defined and precisely controlled thermal and flow conditions. In this final part of a series of papers on PP-300/6, we complement our previous in-situ rheooptical and ex-situ microscopy by using synchrotron SAXS and WAXD to track the evolution of crystalline microstructure during and after the imposition of flow. On the basis of these data and those from the rheooptical and microscopy studies, a model emerges that captures mechanistic aspects of nucleation and growth of oriented crystals under the influence of flow as a function of shearing conditions and crystallization temperature.

The effects of flow on polymer crystallization are highly nonlinear.[6] Thus, to be able to understand morphological development under processing conditions, it is necessary to access the high stresses and strains that are typical of most processing operations. However, it is difficult to develop a fundamental understanding of flow-enhanced crystallization based on crystallization experiments in conventional processing equipment. Data from such experiments are very difficult to interpret due to the complicated thermal and flow histories experienced by the crystallizing polymer. For example, during injection molding, the crystallizing polymer experiences spatially dependent levels of stress and total accumulated strain.[7,8] Further, processing operations are typically nonisothermal,[9] and crystallinity develops as a polymer melt cools, for example, during film blowing[10,11] and injection molding.[8,12,13]

Thus, there is a clear need for experiments that access well-defined processing-like stresses and strains but that separately characterize the roles of flow history and crystallization temperature. Further, to understand the complex interplay of melt relaxation dynamics and crystallization, it would be advantageous to monitor structure development as it happens, in-situ, and to interpret these measurements together with ex-situ microstructural analysis.

Studies using multiple structural probes to characterize order at various length scales are sparse. A few groups have combined in-situ X-ray scattering with electron microscopy to examine polymer crystallization under quiescent or near-quiescent conditions[14−16] or under the influence of flow.[17−20] Recent work by Pople et al.[17] examined structural development in polyethyl-

† California Institute of Technology.
‡ State University of New York.
§ Present address: Division of Polymer Chemistry, National Chemical Laboratory, Pune 411008, India.
* To whom correspondence should be addressed: e-mail jak@caltech.edu; Tel (626) 395-4138; Fax (626) 568-8743.

10.1021/ma035840n CCC: $27.50
Published on Web 10/27/2004

ene subjected to shear under isothermal conditions, using a combination of in-situ WAXD and ex-situ TEM. They found that a high degree of orientation was observed in the final morphology when the polymer melt was subjected to a shear rate above a critical value. They noted that the formation of row nucleated structures observed in the TEM depends on the molecular weight distribution in the sample. Hsiao and coworkers[18−20] have used a combination of SAXS and WAXD to examine crystallization of isotactic polypropylene sheared at a constant rate in a Linkam shear cell. Their investigations revealed that shear promoted the formation of the β-modification.

We have adopted the "short-term" shearing protocol of Liedauer et al.[6,21−23] in which the thermal pretreatment creates a well-defined and reproducible initial condition for the experiment, while the imposition of a brief pulse of shear (for a duration $t_s \ll$ time taken for quiescent crystallization) minimizes the reorientation of crystallites in the flow field and creates a well-defined and reproducible flow history. Shear stresses as high as those typically encountered in polymer processing can be imposed. Thus, the thermal transients and gradients that complicate the interpretation of experiments done using conventional processing equipment are avoided. The flow device constructed in our laboratory[2] retains the key features of the design of Liedauer et al.[6] and incorporates some improvements: (i) the sample requirement has been significantly reduced (to ≈0.5 g/experiment), and (ii) we have added the ability to use several in-situ probes of structure to characterize the development of crystallinity at all the length scales of interest.

Our rheooptical studies[3] of the shear-enhanced crystallization of a polydisperse Ziegler−Natta isotactic polypropylene, PP-300/6 (M_w∼ 300 000 g/mol, polydispersity index, PDI, ∼ 6−8, pentad content [mmmm] ∼ 96%, melt flow index = 12 dg/min at 230 °C/2.16 kg load), indicate that while short-term shearing always accelerates the rate of crystallization, strongly anisotropic skin-core morphologies develop only above a critical level of shearing (viz. only above a critical shear stress and above a stress-dependent critical strain). Further, the effect of shear on the development of the skin appears to saturate beyond a certain shearing duration. Ex-situ optical micrographs[3] and TEM[4] show that the skin is comprised of row-nucleated "shish-kebab" structures (similar to those observed in the skin of injection-molded articles) which are templated by the linelike precursors formed during flow. Interestingly, the temperature dependence of the formation of these linelike precursors reveals that nucleation during flow-induced crystallization is mediated through a rheologically controlled kinetic pathway.[5] These results have been summarized in a recent review.[24]

The following examination of real-time development of crystallinity during and after shearing requires interpretation of SAXS and WAXD integrated across the thickness of the sample in the flow cell. Therefore, it is necessary to appreciate the depth dependence of the semicrystalline structure. Previously published results of optical and electron microscopy[24] provide a real-space image of the morphology and its spatial distribution (e.g., skin-core morphology) at the end of our crystallization experiment. The X-ray data in this paper are analyzed using models based on this final morphology and provide insights into the inception of the microstructure and its evolution to that observed in the micrographs.

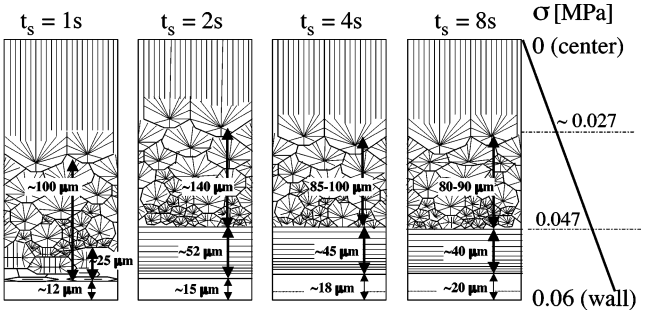

Figure 1. Schematic diagram summarizing the combined results of optical microscopy and electron microscopy images in the flow-velocity gradient plane, showing the evolution of the final semicrystalline microstructure with increasing shearing duration for T_{cryst} = 141 °C and σ_w = 0.06 MPa. The morphology observed for t_s = 8 s is also representative of the structure following shearing for t_s = 12 s.

The progression of the final solid-state morphology as a function of the duration of shearing at fixed temperature and wall shear stress (T_{cryst} = 141 °C, σ_w = 0.06 MPa) shows that pointlike or short needlelike precursors are induced where the shear stress exceeds ∼0.03 MPa (Figure 1). Where the stress exceeds a threshold value $\sigma_{crit} \approx 0.47$ MPa, the needlelike precursors observed for short shearing times $t_s \leq 1$ s are elaborated into long, threadlike precursors ("shish") if shear is sustained for 2 s or more. The resulting row-nucleated morphology in the outermost ≈50 μm (i.e., where $\sigma > \sigma_{crit}$) saturates during the first 4 s of shear. (Continued shearing for twice or even three times longer does not significantly change the average distance between shish observed at any given depth, i.e., at any given shear stress.) In this "saturated" morphology the distance between shish ranges from ≈250 nm near the wall ($\sigma \approx 0.06$ MPa) to ≈750 nm near the boundary between the oriented skin and the fine grained layer ($\sigma \approx 0.047$ MPa).

Highly oriented lamellae are found in the oriented skin; thus, in-situ observation of highly oriented lamellar stacks in SAXS or fiberlike diffraction patterns in WAXD are interpreted as revealing the real-time development of the row-nucleated structure (total optical path length of ≈100 μm for X-rays passing through both skin layers). A broad orientation distribution is associated with the growth propagating from either pointlike precursors (spherulitic) or from widely spaced, short needlelike precursors (leading to somewhat distorted spherulites that are elongated in the flow direction). Our synchrotron X-ray experiments were terminated at ≈30 min, so the "transcrystalline" layer seen in the central zone of the fully solidified specimens is not probed. (Based on the literature value of the growth velocity, propagation of the growth front to the center of the sample requires a few hours.)

Here we present real-time WAXD and SAXS observations of the formation of these morphologies. We begin by outlining the analysis used to extract structural information from the X-ray data: a shearing condition previously shown to produce a strongly oriented morphology is used to present the analysis. This method is then used to examine the influence of shearing conditions (wall shear stress, shearing duration, and crystallization temperature) on the development of semicrystalline morphology. Finally, we examine the implications

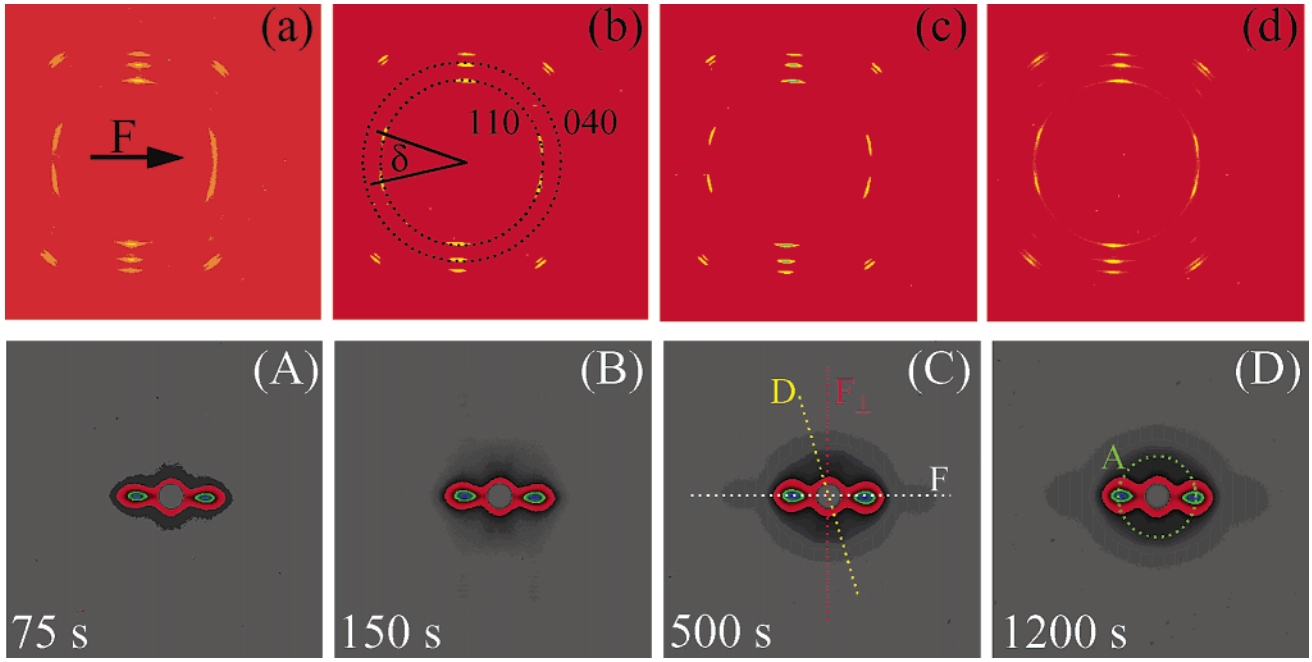

Figure 2. Two-dimensional WAXD (top row) and the corresponding SAXS (bottom row) patterns showing the evolution of crystallinity with time, t_{cryst}, after cessation of shear for $T_{cryst} = 141$ °C and $\sigma_w = 0.06$ MPa, $t_s = 12$ s. The flow direction is horizontal (indicated for the WAXD at 75 s). The development of lamallae with normals along the flow direction (F), along the daughter lobes (D), and perpendicular to the flow ($F_\perp$) is examined by analyzing the SAXS intensity along the respective directions.

of the combination of in-situ rheooptics and X-ray scattering with ex-situ microscopy for a mechanistic description of semicrystalline microstructure development in polymers subjected to flow.

2. Experimental Section

The effects of wall shear stress (σ_w), shearing duration (t_s), and crystallization temperature (T_{cryst}) on development of semicrystalline morphology are studied using the short-term shearing approach.[6,21] In the experiments described here, the polymer was initially held at $T_{relax} = 225$ °C (above the equilibrium melting temperature for iPP, 208 °C) for 5 min to erase its previous thermal and flow history.[3] The melt is then cooled to the desired crystallization temperature and held isothermal thereafter. Once the sample is at T_{cryst}, the relaxed, subcooled polymer melt is subjected to pressure driven flow through a rectangular slit at a wall shear stress, σ_w, for a brief shearing duration, t_s. We use in-situ synchrotron X-ray scattering to probe the development of semicrystalline order: both SAXS and WAXD are employed to elicit detailed structural information about the extent of crystallization and its orientation.

The experimental setup for the synchrotron WAXD measurements has been described previously.[4] Our shear cell, modified for the scattering experiments, has a conical aperture to enable observation of scattered X-rays to angles (2θ) of up to 35°, and the apertures are sealed with 300 μm thick beryllium windows. The shear device is placed on a translation stage for ease of alignment. A liquid-cooled two-dimensional CCD detector (MAR-CCD) with a resolution of 1024 × 1024 pixels (pixel size = 128.8 μm) is used to acquire data for both small- and wide-angle experiments. An α-alumina NIST standard is used to calibrate the scattering angle for WAXD, while a silver behenate standard is used for SAXS. The CCD is placed about 16 cm from the shear cell for the WAXD measurements. For the SAXS, the CCD is placed at a distance of about 105 cm from the shear cell, and an evacuated chamber is used between the shear cell and the CCD to reduce air scattering.

All the synchrotron X-ray scattering experiments were conducted at beamline X-27C of the National Synchrotron Light Source (NSLS), at the Brookhaven National Laboratory, using a wavelength of 0.1307 nm.

3. Results

We begin this section with a detailed examination of synchrotron SAXS and WAXD data that trace the evolution of semicrystalline microstructure during oriented crystallization induced by a particular shearing condition that has been previously determined[3,4] to give rise to an anisotropic skin-core morphology ($T_{cryst} = 141$ °C; $\sigma_w = 0.06$ MPa; $t_s = 12$ s). The method of analysis used to extract structural parameters is outlined, setting the stage for investigating the effects of shearing conditions (σ_w, t_s, and T_{cryst}) on the time course of morphological development.

Upon subjecting PP-300/6 to conditions severe enough to induce the formation of skin-core morphology, the crystallization kinetics are tremendously accelerated; highly oriented WAXD and SAXS patterns develop in a matter of seconds (Figure 2) at a temperature at which the characteristic time for quiescent crystallization (based on rheooptical data[3]) is $t_Q \approx 10^4$ s. The two-dimensional WAXD patterns indicate the formation of a bimodal population of crystals unique to the α crystal form of isotactic polypropylene-consisting of parent lamellae (showing c-axis orientation along the flow direction) and their associated epitaxial daughter lamellae. The strong fiberlike orientation distribution of the crystals generated during flow is perpetuated as the polymer crystallizes after cessation of flow (Figure 2d, top row, $t_{cryst} = 1200$ s; this has been analyzed in detail in a previous publication).[4]

Under these shearing conditions, the SAXS also develops a highly oriented pattern with lobes along the flow direction (Figure 2, bottom row). Faint second-order peaks along the flow direction can be observed for data acquired over long acquisition times (viz. improved signal-to-noise ratio; Figure 2c,d, bottom row), indicating the high degree of ordering of the oriented parent

lamellae. Weak lobes due to scattering from the daughter lamellae can also be observed in the SAXS at about 80° to the flow direction. During the initial stages of crystallization, data are acquired with a time resolution of 10 s. Given this resolution, the development of SAXS and WAXD appears simultaneous.

Analysis of the SAXS Data. Structural information can be extracted from the two-dimensional SAXS patterns by analyzing sections along different directions of interest: for example, the development of lamellar stacks with normals along the flow direction can be probed by examining a section in that direction, i.e., $I(q)$ along the line marked F in Figure 2c, bottom. Similarly, we also examine sections along the direction perpendicular to flow ($F_\perp$) and along the lobes from the daughter lamellae (D). Because of the overlap between the daughter lobes, there is no substantial difference between analysis of data along $F_\perp$ and D. Our data at various shearing conditions span the entire range of orientation from near-isotropic to the fiberlike orientation observed in Figure 2d. For near-isotropic patterns, analysis along sections in the F and $F_\perp$ directions is inappropriate. Rather, the two-dimensional SAXS pattern should be reduced to one dimension by circularly averaging over the azimuthal angle (I_P) and applying the Lorentz correction (q^2I_P). For a sample with a truly isotropic distribution, this azimuthal average would correspond to a "powder" pattern; hence, in our work, we refer to I_P as a "powder" average. Thus, here I_P refers merely to an azimuthal average and does not imply rotation of the sample to obtain a true powder pattern. As our data often lie between the two extremes of isotropic and fiberlike orientation, we analyzed all our data using both the sections along the directions of interest as well as the powder pattern, I_P, and compared the results of these analyses.

Analyses of the correlation function[25] or the interface distribution function[26,27] have been used in the literature[28,29] to obtain detailed structural information regarding the thickness of crystalline and amorphous stacks and the nature of the crystal−amorphous interface. However, these methods typically assume a lamellar stack morphology with variation of electron density along one dimension. Applying these methods of analysis to the α-form of isotactic polypropylene is complicated since the one-dimensional model is not applicable to the crosshatched morphology.[30] However, information regarding the Bragg long spacing and the invariant can be conveniently extracted[31,32] from our data.

The position of the maximum in the SAXS intensity (q^*) is used to determine the long spacing, L_B ($= 2\pi/q^*$). As an example of our analysis we present data acquired at $t_{cryst} = 3250$ s (Figure 3). As expected, the long spacing determined from the Lorentz-corrected powder pattern is shifted to a lower value ($L_{B,P} = 25.4$ nm) compared to the uncorrected powder pattern ($L_{B,U} = 29.2$ nm). From the sections along the F, $F_\perp$, and D directions (plotted on the same scale as each other), it is obvious that the SAXS peak intensity is much stronger along the F direction and, therefore, dominates the powder-averaged pattern. Thus, the value of L_B obtained from an analysis of the F section ($L_{B,F} = 28$ nm) is similar to that from the uncorrected powder pattern. Since the intensity of the SAXS peak along the $F_\perp$ and D directions is comparable to the intensity around the beamstop, the peaks are not well resolved; consequently, the uncertainty in our estimate of $L_{B,D} =$ 28.9 nm along $F_\perp$ and D is large. The long spacing of the daughter lamellae is not distinguishable from that of the parent lamellae ($L_{B,D} \approx L_{B,F} \approx L_{B,U}$). As the polymer crystallizes after shear, the L_B values from the Lorentz-corrected powder pattern and from the F section both remain essentially constant (Figure 3, inset), indicating that the lamellar stacks formed during shear have the same long spacing as those that grow in a quiescent melt at T_{cryst}.

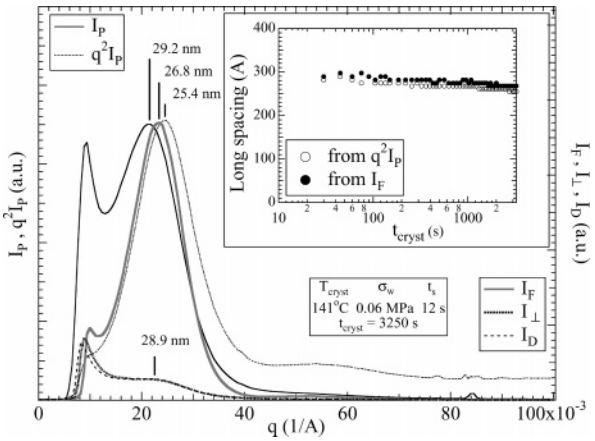

Figure 3. Lamellar long spacing calculated from the powder average, the Lorentz-corrected powder patterns, as well as from sections along F, D, and $F_\perp$ (defined in Figure 1) for data acquired at $t_{cryst} = 3250$ s ($T_{cryst} = 141$ °C, $\sigma_w = 0.06$ MPa, $t_s = 12$ s). The inset shows that the long spacing from the Lorentz-corrected powder pattern and from the section along the flow direction are in good agreement and are nearly constant over the crystallization time, t_{cryst}.

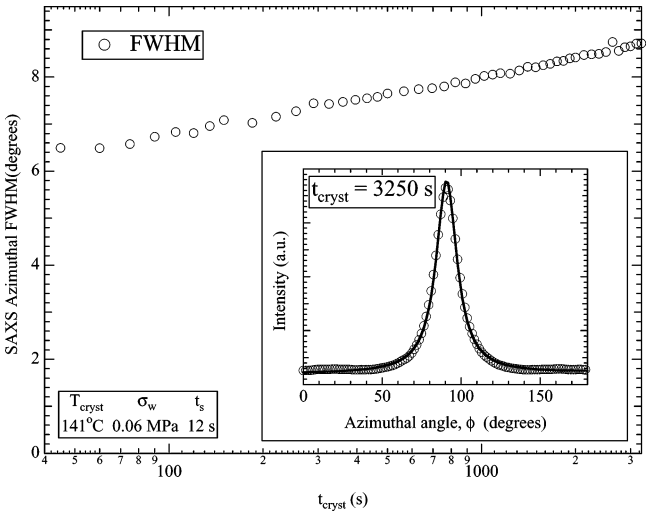

Figure 4. Full width at half-maximum, fwhm, calculated from the azimuthal intensity of the SAXS at the peak value, q^*, increases gradually as a function of the crystallization time ($T_{cryst} = 141$ °C, $\sigma_w = 0.06$ MPa, $t_s = 12$ s). The inset shows an example of the Lorentzian fit to the SAXS azimuthal scan acquired at $t_{cryst} = 3250$ s.

The SAXS patterns can also be used to obtain an estimate of the orientation distribution of the crystalline lamellae by examining the azimuthal intensity at the peak radial value. A Lorentzian peak shape was determined to give a good fit to the azimuthal data (Figure 4, inset shows an example of the fit). The full width at half-maximum (fwhm) obtained from the fit increases slightly and gradually from about 6° to 8°, indicating that threadlike precursors generated during shear template with high fidelity the orientation of lamellae

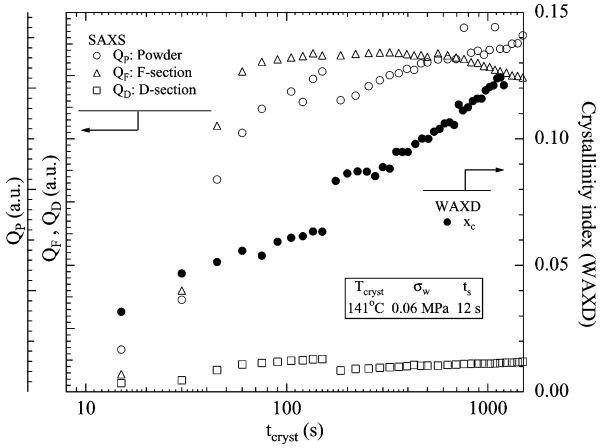

Figure 5. Comparison of the SAXS invariants from the Lorentz-corrected powder pattern, Q_P, and from directions along the flow and daughter sections (Q_F and Q_D, respectively) with the crystallinity index computed from the WAXD, x_c (T_{cryst} = 141 °C, σ_w = 0.06 MPa, t_s = 12 s). The trends in x_c parallel those for Q_P, except that the rate of increase beyond 100 s is steeper for WAXD than for SAXS.

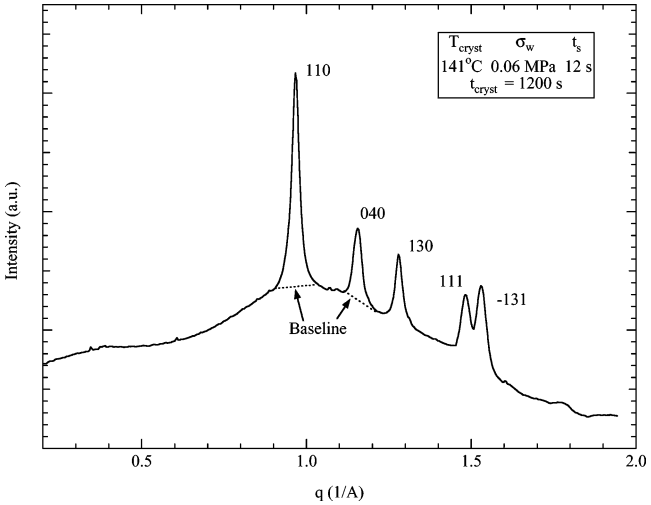

Figure 6. Circularly averaged WAXD powder pattern with the crystalline peaks indexed for T_{cryst} = 141 °C, σ_w = 0.06 MPa, t_s = 12 s at t_{cryst} = 1200 s. The "amorphous" value of the baseline is indicated for the 110 and 040 reflections.

that grow laterally from them both during and after shear.

Having examined the geometrical aspects of the morphology such as the long spacing and degree of orientation, we now focus on the SAXS invariant, $Q = \int_0^\infty I\, dq$, where I is either the intensity along the F, $F_\perp$, or D sections, or the Lorentz-corrected intensity of the circularly averaged powder pattern (Figure 5). For a spatially inhomogeneous lamellar two-phase sample such as in our experiment, Q is proportional to $\langle x_l(1 - x_l)\Delta\rho^2\rangle$, where x_l is the *local* crystallinity, $\Delta\rho$ is the electron density difference between the crystal and amorphous phases, and $\langle ...\rangle$ represents a spatial average over the scattering volume.[33,34] To calculate the invariant, data are extrapolated linearly[29] to 0 at low q and using Porod's law[33,34] in the limit $q \to \infty$. According to Porod's law

$$\lim_{q\to\infty} q^4(I - I_l) = K \tag{1}$$

where I is the experimental SAXS data, I_l is the liquid scattering, and K is the Porod constant. For our data, we obtain a good fit by assuming that I_l does not have a q dependence.

The invariant calculated from the F section, Q_F, rises sharply over the first 100 s of crystallization and then remains approximately constant to about 1000 s, after which it shows a gradual decrease. Based on ex-situ microscopy (summarized in Figure 1), lamellae that are strongly oriented along the flow direction are localized in a thin, row-nucleated layer (~55 μm thick near each wall); thus, the rapid increase in Q_F during the first 100 s indicates that the row-nucleated structure grows to impingement in ~1% of the quiescent crystallization time at this temperature. The slow decrease in Q_F at longer t_{cryst} might be due to development of crystallinity in the interlamellar regions (Q shows a maximum at x_l = 0.5 and decreases for higher x_l) or densification of the daughter lamellae which would lead to a decrease in the effective $\Delta\rho$ within the parent lamellar stacks.[35] The invariant computed from the powder analysis, Q_P, rises quickly over the first 100 s and continues rising at a slower rate thereafter. Analysis of the invariant along the daughter direction, Q_D, is less reliable since the intensity around the beamstop makes it difficult to extrapolate the SAXS data to q = 0. The growth of Q_D shows a similar trend to Q_P, increasing rapidly in the first 100 s and then gradually at longer times. As expected, the magnitude of the Q_D is about an order of magnitude smaller than Q_F due to the irregularities in spacing between the daughter lamellae and the small size of the correlated daughter-stacks.[4] The increase of Q_P and Q_D at large t_{cryst} in contrast to the decrease in Q_F indicates the gradual development of lamellae with a broad orientation distribution. Previous ex-situ TEM[4] indicates that these less oriented crystallites form at greater depth than the oriented skin, toward the center of the shear cell.

Analysis of the WAXD Data. The WAXD crystallinity index, x_c, is calculated from an azimuthally averaged pattern (Figure 6) as follows:

$$x_c = \frac{\int_0^\infty q^2 I_c\, dq}{\int_0^\infty q^2 I\, dq} \tag{2}$$

where I_c is the intensity of the crystalline peaks above the baseline and I is the total scattered WAXD intensity. Intensities of the crystalline peaks were obtained from the WAXD pattern by fitting: the WAXD observed for the melt was used as an "amorphous baseline", and each crystalline peak was represented by either a Gaussian or a Lorentzian line shape chosen by visually determining the quality of the fit. The crystallinity index is dominated by the crystalline peaks at low q values and does not account for distortions of the crystalline lattice that suppress the crystalline intensity at high q values. Further, the "amorphous" halo includes scattering from air and the beryllium windows of the flow cell. Hence, x_c represents a lower bound for the crystallinity.

The crystallinity index increases rapidly to a value of about 0.03 *during* flow and to about 0.06 in the first 150 s and finally to about 0.12 over t_{cryst} = 1200 s. Thus, shear dramatically enhances the rate at which crystals form. During intense shearing, crystals form approximately 10 times as fast as after cessation of shear. In this case, the crystallinity in the skin region at the end of the shear pulse reaches half of the crystallinity at

impingement. From the in-situ WAXD[4] and the ex-situ microscopy,[3,4] we infer that in the initial 150 s crystallites develop only in skin regions near each wall (roughly 55 μm at each wall of the 500 μm shear cell), while very little if any crystallization takes place in the near-quiescent core. Since x_c represents a spatial average over the entire width of the shear cell, the crystallinity developed in the skin at the end of 150 s exceeds 0.27 [$= 0.06 \times 500/(2 \times 55)$].

The WAXD x_c data show an abrupt break at 150 s which is an artifact of the data acquisition system: the first 10 data points (up to $t_{cryst} = 150$ s) were acquired rapidly to capture the sharp initial increase (acquisition time = 10 s/data point), after which longer acquisition times were used to improve signal:noise. However, we observe a slight change in the shape of the amorphous halo in the WAXD after the first stage of data acquisition which is manifested as a break in x_c. We do not know the reason for this change in the shape of the halo.

We examine the intensity at the 110 and 040 peak positions due to diffraction from crystals by subtracting the appropriate baseline value (indicated in Figure 6). The diffraction from the parent and daughter 110 planes are separated in azimuthal angle for the 110 peak but are both at the same azimuthal position (along the meridian) for the 040 peak. The 110 and 040 peaks are fit simultaneously and are constrained so that (i) the ratio of the width of parent peak to the daughter is the same for the 110 and 040 reflections and (ii) the ratio of the areas under the parent and daughter peaks is the same for 110 and 040 reflections (after a geometrical correction for the angle made by the plane normal to the axis of symmetry). We present the data and the fits for the WAXD data at $t_{cryst} = 1200$ s as an example (Figure 7). The data were fitted with a constant baseline value and Lorentzians for each of the parent and daughter peaks. The baseline represents scattered intensity from the nonoriented crystals while the area under the Lorentzians represents scattering from the oriented crystals. The angular separation between the daughter crystal peaks, $\delta \approx 34°$ (Figures 2b and 7), is lower than the expected value of 38.3° for the idealized case of perfect uniaxial orientation. Such deviations have been explained in the literature[36] to arise due to curving and twisting of crystal lamellae that broaden the diffraction peaks along the azimuthal direction.

The azimuthal widths of the 110 and 040 parent and daughter peaks obtained from the fits remain essentially constant with crystallization time (Figure 8) and compare well with the fwhm obtained by fitting the SAXS azimuthal scans. Further, the amplitude of the Lorentzians fitted to the oriented parent and daughter peaks (which are proportional to the intensity since the widths of the peaks are unchanged with t_{cryst}) increase rapidly and in concert for the first ≈100 s, after which they saturate (Figure 9). On the other hand, the amplitude of the baseline (which is proportional to the fraction of unoriented crystals) increases slowly with time after about 100 s. Thus, the ratio of the baseline value to the area under the oriented parent and daughter peaks, which is a measure of the ratio of the unoriented crystal fraction to the oriented, increases with crystallization time to $t_{cryst} = 1200$ s.

Effects of Shearing Conditions on Crystallization. We begin by presenting two-dimensional scattering patterns for different shearing conditions and then analyze one-dimensional profiles extracted from the

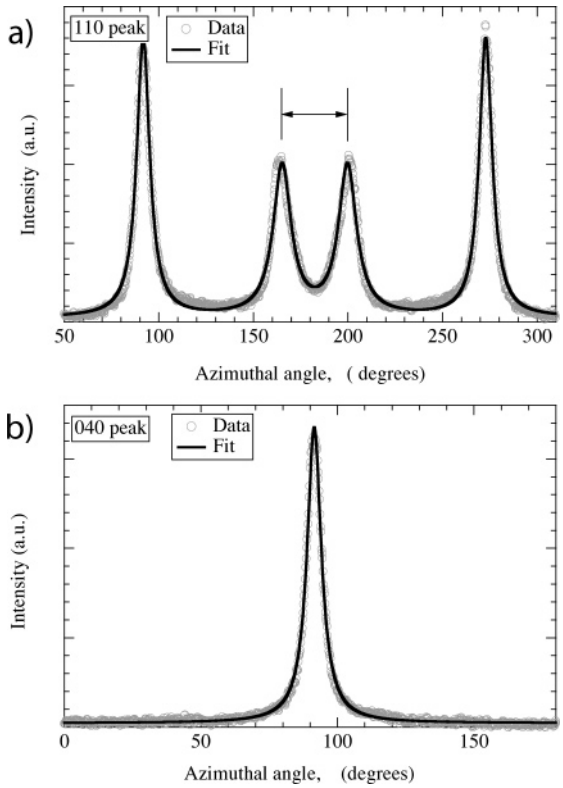

Figure 7. Azimuthal variation of the intensities at the 110 and 040 WAXD peak locations with the appropriate baseline value subtracted with the fit for $t_{cryst} = 1200$ s ($T_{cryst} = 141$ °C, $\sigma_w = 0.06$ MPa, $t_s = 12$ s). The two data sets of the crosshatched peaks, δ (see Figure 1) is ≈34°.

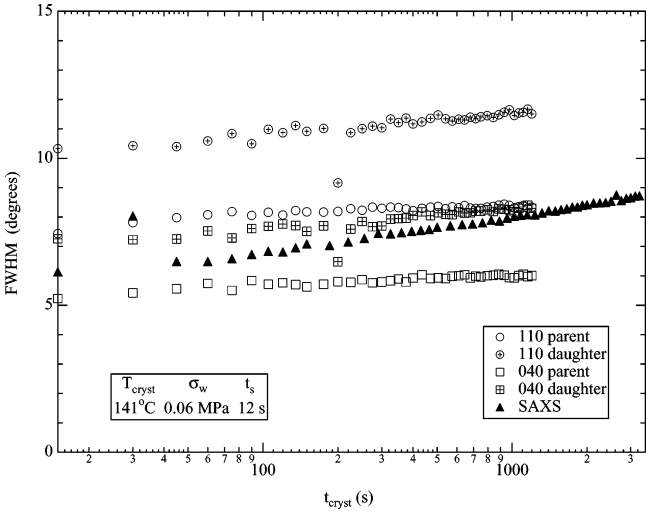

Figure 8. Azimuthal fwhm for the parent and daughter WAXD peaks at the 110 and 040 reflections for $T_{cryst} = 141$ °C, $\sigma_w = 0.06$ MPa, $t_s = 12$ s (determined by fitting, see Figure 6) are very weak functions of the crystallization time, t_{cryst}.

SAXS and WAXD patterns. We focus on the effects of three parameters—shearing duration (t_s), wall shear stress (σ_w), and temperature (T_{cryst})—on the morphology (viz. orientation and ratio of parent to daughter crystals) and on the kinetics of crystallization.

In terms of the effects of shear history on the morphology of crystallization, qualitative trends are evident by inspection of the two-dimensional WAXD and SAXS patterns (Figure 10). Increasing the shearing time increases the degree of orientation while reducing the ratio of daughter to parent crystals. Increasing the

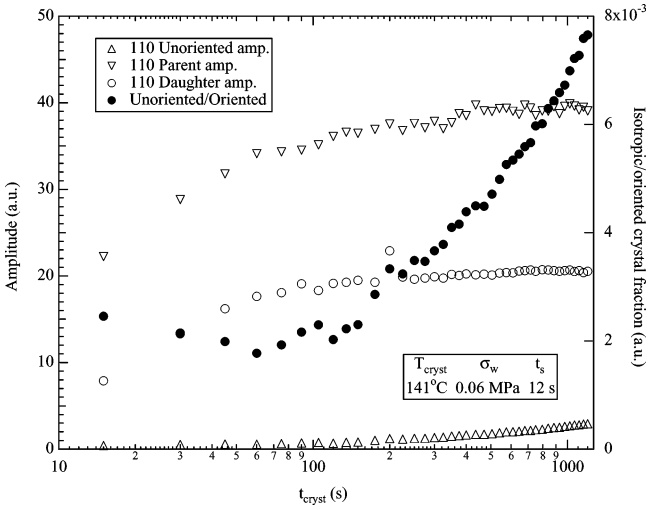

Figure 9. Amplitude of the fits to the parent and daughter 110 peaks and to the unoriented crystal component for T_{cryst} = 141 °C, σ_w = 0.06 MPa, t_s = 12 s.

applied stress from below (σ_w = 0.03 MPa) to above (σ_w = 0.06 MPa) the threshold value for highly anisotropic crystallization ($\sigma_{crit} \approx$ 0.047 MPa at 141 °C[3]) causes the structure to change from a modestly aligned orientation distribution (even for t_s as long as 20 s at σ_w = 0.03 MPa, Figure 10b,B) to strong fiberlike orientation (even for t_s as short as 2 s at σ_w = 0.06 MPa, Figure 10c,C). Increasing the crystallization temperature from 141 to 150 °C for σ_w = 0.06 MPa reduces the ratio of daughter to parent crystals while retaining the strong fiberlike orientation (cf. Figures 10 c,C to e,E and d,D to f,F).

The trends in terms of morphology correlate with associated trends in crystallization kinetics evident in the time evolution of the SAXS and WAXD aximuthal scans presented in Figures 11−14. In view of the effects of shearing time on the final solid-state morphology (Figure 1), the increase in the threadlike precursors with t_s in the thin regions where $\sigma > \sigma_{crit}$ gives rise to more rapid formation of crystallites (Figure 12) as increase in the length of shish per unit volume provides greater area of growth front. When the highest stress in the sample is too low to generate threadlike precursors (no threadlike precursors are evident at a depth of 125 μm in Figure 1 where the shear stress is 0.03 MPa, equal to the wall shear stress imposed the experiments shown in Figure 13), the kinetics and orientation distribution resemble those seen at higher stress for t_s so short that threadlike precursors have not yet formed (cf. Figure 12b and Figure 13b). Although final solid-state structure was only examined for T_{cryst} = 141 °C, trends with shearing duration are the same for experiments at higher T_{cryst} (cf. Figure 14 at T_{cryst} = 150 °C to Figure 13), suggesting that the formation of thread-

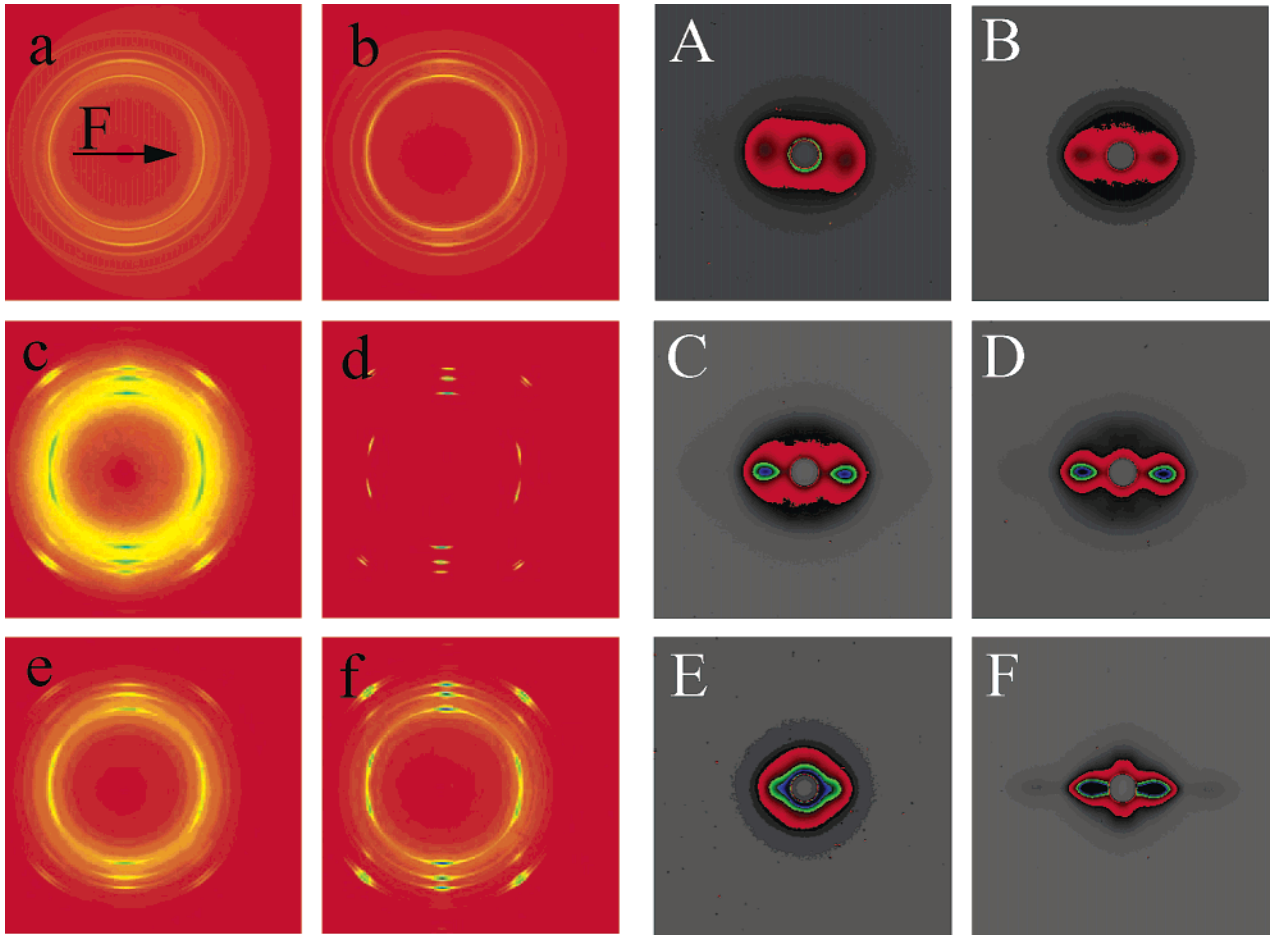

Figure 10. Two-dimensional SAXS alnd WAXD patterns showing the influence of σ_w, t_s, and T_{cryst} on crystallization. The last patterns acquired for each experiment are shown (ranging from 1200 to 7300 s, depending on the conditions—see Figure 15 for the duration of each experiment). Two temperatures are examined: T_{cryst} = 141 °C (a−d, A−D) and 150 °C (e,f, E,F). At 141 °C results are shown for two wall shear stresses: σ_w = 0.03 MPa for relatively brief shearing of t_s = 1−2 s (a [2s], A [1s]) and longer shearing t_s = 20 s (b, B), and 0.06 MPa for t_s = 2 s (c, C) and t_s = 20 s (d, D). At 150 °C, only the higher shear stress σ_w = 0.06 MPa is examined, comparing t_s = 1 s (e, E) with t_s = 6−8 s (f [8s], F [6s]).

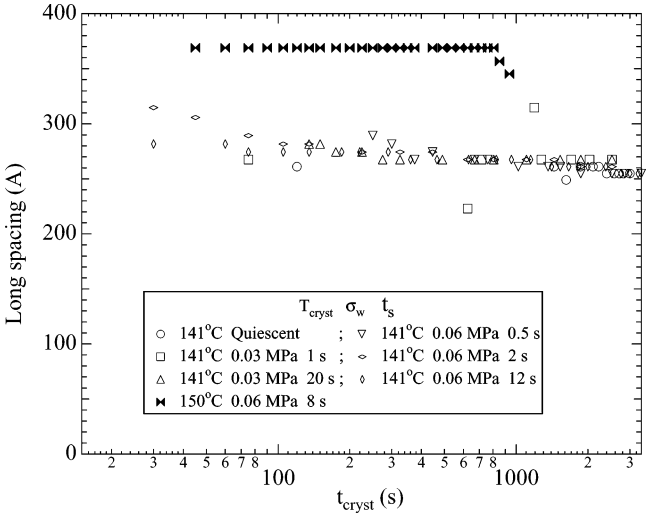

Figure 11. SAXS long spacing. The lamellar spacing at a particular T_{cryst} does not change for sheared samples compared to the value for quiescent crystallization.

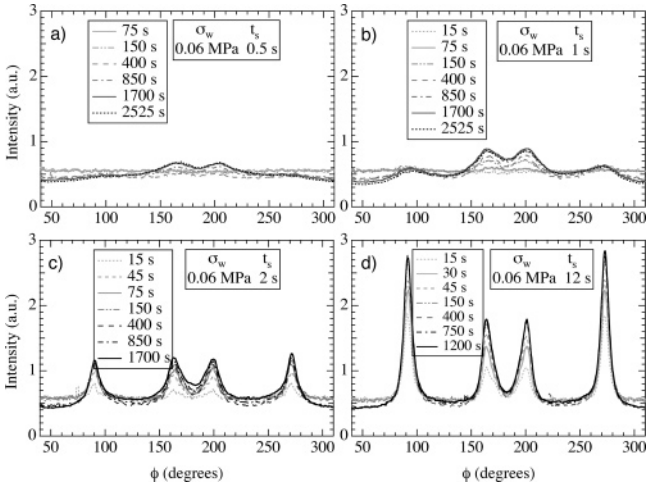

Figure 12. Evolution of azimuthal intensity at the 110 WAXD peak with crystallization time for t_s = 0.5, 1, 2, and 12 s at T_{cryst} = 141 °C and σ_w = 0.06 MPa.

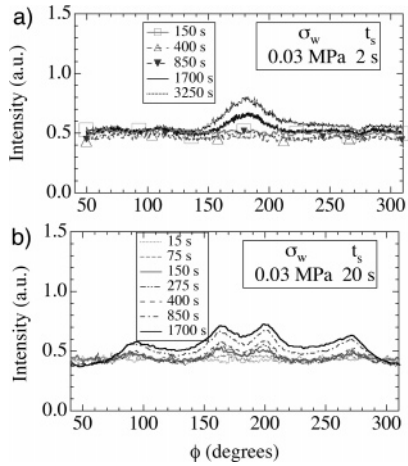

Figure 13. Evolution of azimuthal intensity at the 110 WAXD peak with t_{cryst} for t_s = 2 and 20 s at T_{cryst} = 141 °C and σ_w = 0.03 MPa. For clarity, the curves shown for 150, 400, and 850 s are smoothed, with symbol sizes indicative of the amplitude of the noise.

like precursors progresses with shearing time in a similar manner at 150 °C as at 141 °C, in accord with the previous report of a kinetic pathway to oriented

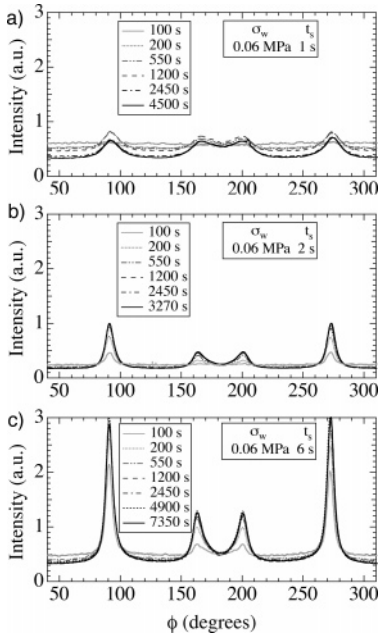

Figure 14. Evolution of azimuthal intensity at the 110 WAXD peak with crystallization time for t_s = 1, 2, and 6 s at T_{cryst} = 150 °C and σ_w = 0.06 MPa.

precursors.[5] The formation of threadlike precursors does not appear to be controlled by either total strain or total work: while the total strain at the wall, γ_{tot}, is approximately 100 for t_s = 20 s at σ_w = 0.03 MPa, the total strain for t_s = 1 s at σ_w = 0.06 MPa is only about 10.[5] The method to determine the approximate strain is given in the Supporting Information of reference 5.

The nanostructure of the lamellar stacks is primarily determined by the crystallization temperature. SAXS long spacing, L_B, is unaffected by σ_w and t_s: it remains essentially constant at the same value as for quiescent crystallization at a given T_{cryst} (Figure 11). As T_{cryst} is increased from 141 to 150 °C, L_B increases, as expected. The value of L_B at 150 °C is at the upper limit of what can be calculated using our program (37 nm). Increasing T_{cryst} also decreases the ratio of daughter to parent crystals (cf. Figure 12d, t_s = 12 s for 141 °C/0.06 MPa, and Figure 14c, t_s = 6 s for 150 °C/0.06 MPa). This trend in daughter-to-parent ratio accords with literature reports of decreasing the density of crosshatches with temperature.[37−40]

We now examine the orientation distribution and parent:daughter ratio using azimuthal scans at the 110 and 040 WAXD peaks. The peaks in the azimuthal scans were fitted with Lorentzians, and the fwhm was used to quantify orientation. For shearing times too short to induce strong orientation ($t_s \leq$ 1 s at 141 °C, for σ_w = 0.06 MPa, Figure 12a,b), the 110 peaks are too broad to determine the fwhm.[41] Once strongly oriented growth is induced, the angular distribution of the oriented crystal population is largely established during the shearing duration and varies weakly if at all after cessation of flow. For t_s = 2 s, the 110 peaks for the parent crystallites have a fwhm that increases gradually from 10° to 13° over approximately 2000 s (Figure 12c), and for t_s = 12 s, these peaks have a fwhm of only 7−8°, remaining essentially unchanged from 15 to 2000 s (Figure 12d). Azimuthal scans of SAXS at q^* (data not presented) accord with the angular distribution determined from the WAXD pattern, as in the case analyzed in detail above (t_s = 12 s). The ratio of parent to

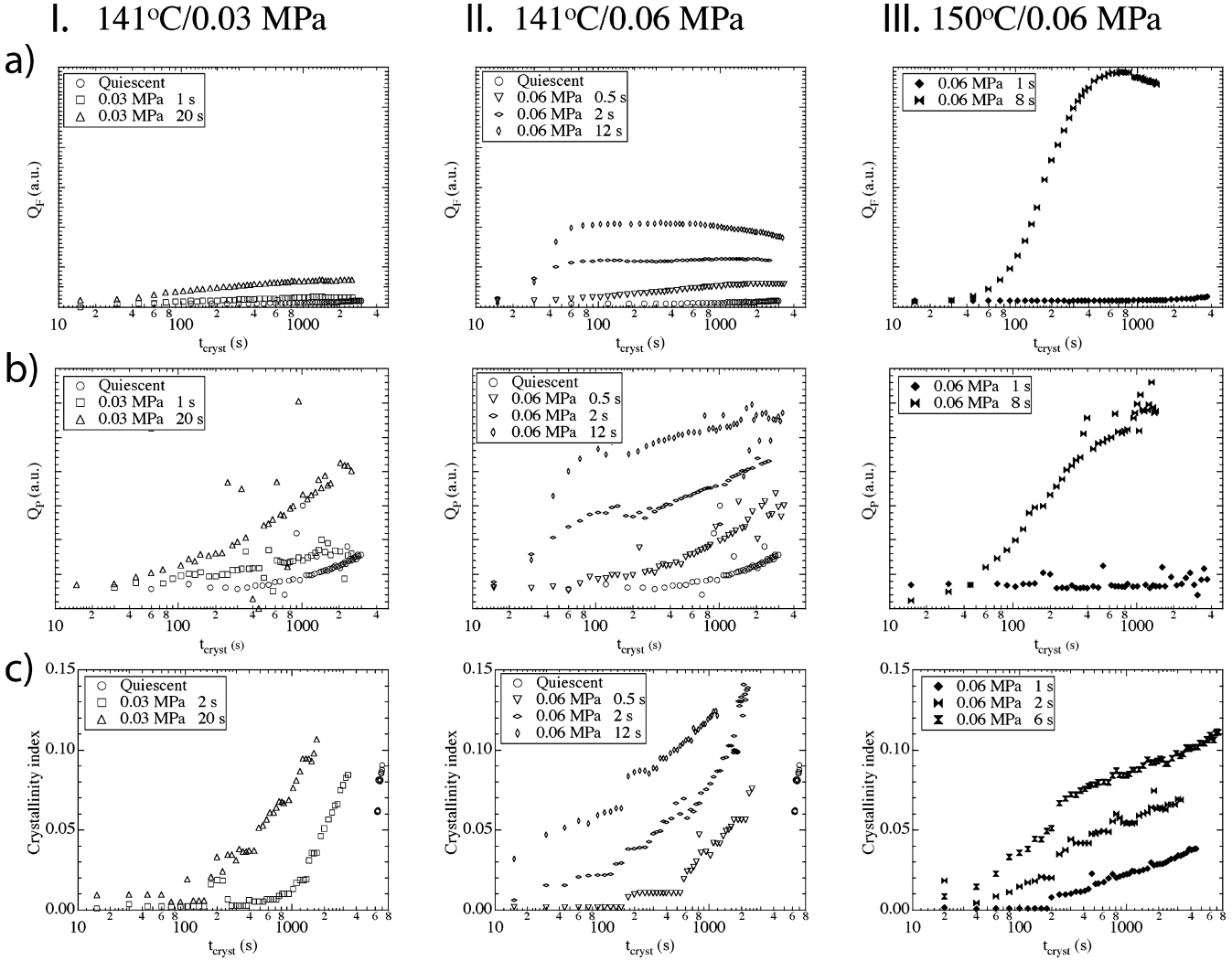

Figure 15. Influence of σ_w, t_s, and T_{cryst} on the evolution of Q_F (first row), Q_P (second row), and x_c (last row): the first two columns show data at 141 °C for $\sigma_w = 0.03$ and 0.06 MPa, respectively; the last column shows data at 150 °C and $\sigma_w = 0.06$ MPa. Note that the arbitrary units used to plot the SAXS invariants are consistent across each row.

daughter crystals associated with the oriented material increases with increasing shearing duration: for $t_s \leq 1$ s, the daughter peaks appear more prominent than the parents; the two sets of peaks have similar heights for $t_s = 2$ s; and for $t_s = 12$ s of shear, the parent peaks are stronger than the daughters. In this most oriented case, an estimate of the ratio of parent to daughter crystallite content to be 3.65 based on the areas of their respective peaks after accounting for a geometrical factor for the angle made by respective crystals to the symmetry axis.[36,42]

It is not possible to quantitatively compare the numerical values of the SAXS invariant Q_P and the WAXD x_c for different shearing conditions even after normalizing the data for acquisition time and incident X-ray intensity due to the effect of the orientation distribution on scattering and due to the change in the ratio of parent to daughter crystals with shearing conditions. Nevertheless, it is instructive to examine various measures of crystallinity following different shearing conditions and compare their relative growth rates. The rate of crystallization is accelerated with increase in t_s (compare Figure 12a with Figure 12d) or σ_w (compare Figure 12d with Figure 13b). The trends in the kinetics remain the same at higher T_{cryst}; however, the ratio of the unoriented crystal fraction to the oriented increases very gradually at 150 °C compared to 141 °C since the quiescent crystallization kinetics slow down by nearly an order of magnitude with the 10° increase in T_{cryst} (compare, for example, Figure 12d with Figure 14c).

The acceleration of the growth of the overall crystallinity vis à vis that of the oriented population can be assessed by examining the transient growth of the SAXS invariants, Q_F and Q_P, and the WAXD x_c (Figure 15). For sufficiently short shearing durations, flow-induced acceleration is roughly isotropic (Q_F and Q_P have similar shapes for the shortest t_s shown for each σ_w and T_{cryst}), consistent with the final solid-state morphology being spherulitic (e.g., Figure 1a,b). With increasing t_s, a separation of time scales emerges, with the oriented crystallites growing rapidly in the early stages and relatively isotropic crystallites growing on much longer time scales. This change is evident in differences in the shapes of $Q_F(t)$ and $Q_P(t)$, e.g., 141 °C, $\sigma_w = 0.06$ MPa, $t_s = 2$ or 12 s or 150 °C, $\sigma_w = 0.06$ MPa, $t_s = 8$ s. During the initial stages, the oriented population rises rapidly and then flattens ($Q_F(t)$ rises and then plateaus), and in the later stages relatively isotropic growth occurs ($Q_P(t)$ continues to rise even after $Q_F(t)$ flattens out). In the early stages, the oriented population dominates the overall population, causing $Q_F(t)$ and $Q_P(t)$ to increase

similarly until Q_F plateaus. The final solid-state morphology shows that the rapid formation of a strongly oriented population correlates with the formation of long threadlike precursors in the oriented skin. During the plateau in Q_F, the overall crystallinity continues to grow in a manner similar to quiescent crystallization (for example, during the Q_F plateau at 141 °C, $\sigma_w = 0.06$ MPa, $t_s = 12$ s, Q_P rises with time at a rate between that of the quiescent case and perhaps double that rate). In the context of the final solid-state morphology, the weakly oriented population reflects spherulitic growth in the core of the sample.

The overall trends in the SAXS invariants and x_c at 150 °C (right column Figure 15) are qualitatively similar to those at lower T_{cryst} (center column, Figure 15). However, there are some interesting differences. The SAXS invariant along the F section (0.06 MPa, $t_s = 8$ s) is considerably higher compared to lower temperature 141 °C (0.06 MPa, $t_s = 12$ s), while the magnitudes of Q_P are comparable in the two cases. This is because at higher T_{cryst} the SAXS peak appears at lower q, and in the Lorentz-corrected powder invariant (q^2I_P), the increase in I_P is offset by the shift to smaller q. The almost 3-fold higher magnitude of the plateau of Q_F at 150 °C than at 141 °C is *not* due to a difference in the degree of orientation (see similarity in Figures 12d and 14c). Instead, the increase in Q_F might be due to the decreased extent of crosshatching at the higher temperature, increasing the effective electron density difference within the parent lamellar stacks. A change in the local crystallinity, x_l, in the lamellar stacks could also play a role. For milder shearing conditions ($t_s = 1$ s), crystallinity does not develop as rapidly as for $t_s = 8$ s, and the proximity of the scattered intensity to the beamstop makes the SAXS peak appear as a shoulder close to the beamstop. This makes it difficult to extract the SAXS invariants since extrapolation of the intensity to low q cannot be done reliably. Thus, $x_c(t)$ provides the most reliable indicator of crystallinity for $t_s = 1$ s at 150 °C, showing a gradual increase with t_{cryst}, while the SAXS invariants show, at best, a very modest increase.

For all other conditions, the qualitative trends in the time course of overall crystallization indicated by Q_P are also evident in x_c, for samples subjected to "strong" shearing the rate of increase of Q_P is slower than that of x_c at longer crystallization times when less oriented crystallization takes place (Figures 5 and 15). The most significant contribution to this effect probably arises from the change in the orientation distribution due to the different orientation dependences of SAXS and WAXD scattering intensity. In the WAXD experiment, uniaxial orientation of α-crystals about their c-axis gives similar average diffracted intensity to an isotropic distribution. (Relative to the isotropic case, the uniaxial distribution shows a 10−30% decrease in intensity[43] from the most significant WAXD peaks, the 110, 040, 130, 111, and −131 reflections.) However, for SAXS, the scattering intensity from lamellae arranged such that all their normals are along the flow direction is much greater than for lamellae with their normals distributed isotropically. Thus, as a weakly oriented population of crystals begins to grow, the relative increase in the SAXS powder invariant, Q_P, is smaller than the increase observed for the WAXD x_c.

4. Discussion

Synchrotron X-ray results reveal in real time the influence of shearing conditions on the rate and anisotropy of crystallization in the oriented skin and spherullitic core present in the final semicrystalline morphology. Under conditions that lead to distorted spherulitic morphologies ($\sigma_w < \sigma_{crit}$ or very small t_s at $\sigma_w > \sigma_{crit}$), SAXS and WAXD provide information regarding the creation of pointlike precursors and the growth of crystallites from them. Experiments at $\sigma_w = 0.06$ MPa ($>\sigma_{crit}$) with longer shearing times ($t_s \geq 2$ s) provide information about the creation of the threadlike precursors and the propagation of the growth front out from them. Furthermore, experiments with $\sigma_w = 0.03$ MPa provide information regarding the contribution of the interior of the sample to the signal observed in experiments with $\sigma_w = 0.06$ MPa at the same T_{cryst} and similar t_s.

Flow conditions that enhance the formation of pointlike precursors, but are too gentle to induce a row-nucleated morphology, generate structures during flow that are too dilute to detect with either SAXS or WAXD in the present experiments. Their presence is manifested several seconds after cessation of flow, when crystals are observed growing on time scales at which quiescent growth would not be detectable. Furthermore, when growth is detected, it is not isotropic, as would be the case for quiescent growth (or for truly "pointlike" precursors). For $\sigma_w = 0.06$ MPa, at shearing times too short to induce the row-nucleated morphology ($t_s = 1$ s, Figure 12), the 110 peak shows enhanced intensity in the angular range that corresponds to the parent and daughter peaks in the row-nucleated structure ($t_s = 2$ or 12 s, Figure 12). Because of the higher intensity associated with the daughter crystallites (simply due to their orientation), even for the shortest shearing time investigated, an enhancement of the 110 intensity in the angular range associated with the daughter peaks is evident. The orientation distribution seen for $\sigma_w = 0.03$ MPa applied for 0.5 s (Figure 13) shows a similar enhancement in the region of the daughter peaks, but with a sufficiently broad azimuthal range that the peak intensity arises from the overlap between them. This bias in the orientation distribution is also seen in SAXS, in which the relative enhancement due to flow is greater for Q_F than for Q_P (e.g., for $t_s = 0.5$ s at $\sigma_w = 0.06$ MPa, Q_F is enhanced 5-fold relative to quiescent crystallization, while Q_P is only roughly doubled). Therefore, the WAXD and SAXS results reinforce the morphological evidence from TEM, indicating that the initial enhancement of nucleation due to flow induces precursors that can be viewed as short needles that are preferentially oriented along the flow direction.

This evidence for needlelike precursors is borne out in the time evolution of the azimuthal WAXD profiles for $\sigma_w = 0.03$ MPa (Figure 13). For the shorter shearing time ($t_s = 2$ s, Figure 13), the orientation distribution is so broad that the daughter peaks fully overlap and the parent peaks are not perceptible, as would be expected if the needles are so short that they nearly approximate "pointlike" precursors. For the longer shearing time ($t_s = 20$ s, Figure 13) the degree of orientation is much stronger (daughters are well-resolved azimuthally and parent peaks with c-axis along the flow are clearly seen), as would be expected for longer needles. With increasing time after cessation of shear, the orientation distribution broadens and the relative contribution of the unoriented population increases. Moving away from the wall of the shear cell toward the center, the local shear stress during flow

decreases, so the needles are shorter and less densely nucleated (see TEM presented in a previous publication).[24] Hence, we expect that these form increasingly isotropic crystallites that continue to grow after impingement of the oriented crystals near the wall. Growth outward from an isolated needle also gives rise to a broader orientation distribution with time: for crystals growing with the same growth velocity (equal to the quiescent value), the volume of the crystals growing from the ends increases as r^3 while the volume of oriented crystals grows as r^2, where r is the distance the growth front has propagated from the precursor. Thus, the broadening of the orientation distribution with increasing t_{cryst} observed from WAXD accords with the final morphology observed by TEM.[24]

The needlelike nuclei that form following inception of flow are elongated during continued shearing at $\sigma_w > \sigma_{crit}$. Thus, highly anisotropic nuclei are formed for intense shearing conditions ($\sigma_w = 0.06$ MPa, $t_s > 2$ s) while shorter needles are formed at $\sigma_w = 0.03$ MPa and for $t_s < 2$ s at $\sigma_w = 0.06$ MPa.[24] Upon cessation of shear, the polymer melt relaxes rapidly and subsequent crystal growth happens under quiescent conditions. Thus, for the shorter needle nuclei, crystal growth is similar to that under quiescent conditions: the growing crystallites undergo noncrystallographic branching, leading to the formation of near-spherulitic structures as the crystals grow. The highly anisotropic needles or threadlike precursors that form under intense shearing conditions act as highly effective nuclei and nucleate the dense growth of lamellae radially outward from the cylindrical core. These radial lamellae are closely spaced and cannot branch and splay. Only the lamellae that originate near the ends of a "shish" can splay due to noncrystallographic branching. Thus, long threadlike precursors template oriented crystals that give rise to the observed fiberlike diffraction patterns that increase in intensity until the cylindrulites impinge.

The effect of shear stress on crystallization is highly nonlinear. A comparison of the azimuthal WAXD profiles at $T_{cryst} = 141$ °C for $\sigma_w = 0.03$ MPa, $t_s = 20$ s (Figure 13, bottom) with $\sigma_w = 0.06$ MPa, $t_s = 1$ s (Figure 12) shows that doubling the stress in this range has such a great effect that even a 20-fold greater shearing time at the lower shear stress cannot induce comparable orientation or acceleration of the rate of crystallization. This accords well with the literature[44] as well as with our earlier rheooptical measurements.[3]

The parent-to-daughter ratio is strongly influenced by the crystallization temperature and by the imposed flow. With increase in temperature, fewer daughter crystals are formed, as expected.[45] There is also an increase in the ratio of parent to daughter lamellae (azimuthal 110 scans, Figure 13), with increase in shearing duration. White and Bassett[38] have demonstrated that, under quiescent conditions, the degree of crosshatching and the thickness of the crosshatched lamellae are independent of the anisotropy of nucleation—hence, the enhanced parent-to-daughter ratio cannot be explained by the orientation of the line nuclei. We speculate that the increase in the parent:daughter ratio with shearing duration arises due to flow-enhanced nucleation and growth of crystallites with *c*-axis along the flow, enhancing the parent crystals compared to the daughters. Crystals formed after cessation of flow are expected to form with the parent:daughter ratio typical of quiescent crystallization at T_{cryst}, since the stresses relax very rapidly after cessation of flow. With increasing times after cessation of flow (viz. when $t_{cryst} \gg t_s$), the parent:daughter ratio decreases as suggested by this explanation (Figure 12d). As a considerable fraction of the crystallization in the skin develops during flow (especially for "strong" shearing), the enhanced parent:daughter ratio during flow skews the overall ratio in the final semicrystalline structure.

The influence of shearing condition on the parent:daughter ratio might also explain the anomalously low birefringence observed in our rheooptical experiments[3] for less intense shearing conditions (viz. $\sigma_w < \sigma_{crit}$ or very short t_s, say $t_s < 2$ s at $\sigma_w = 0.06$ MPa and $T_{cryst} = 141$ °C). Under these shearing conditions, TEM[24] shows that the crystallites formed are anisotropic and would be expected to be birefringent. However, the WAXD data reveal that milder shearing conditions do not reduce the population of daughter crystals relative to the parents. These daughter crystals grow approximately perpendicular to the parents and hence could largely cancel out the birefringence contributed by the parents. Under intense shearing conditions, we observe a highly birefringent structure during shear that correlates well with the formation of oriented crystals observed in WAXD.[5]

The large drop in birefringence observed immediately after cessation of shear in our rheooptical experiments[3] can also be interpreted using the WAXD data. While the birefringence drops, there is no significant change in the observed WAXD pattern. Hence, the drop in birefringence is *not* due to a broadening of the orientation distribution of the crystallites or to a decrease in the degree of crystallinity. Instead, the decrease in birefringence must result from the amorphous part of our sample. However, the observed birefringence is much greater than the steady-state flow birefringence of the melt alone. We speculate that the large birefringence drop is due to the elastic "snapping back" of polymer molecules that are tethered to the scaffold formed by the crystalline precursors. The rapid decay of the birefringence is in good accord with the time scales for stress relaxation expected at these temperatures.

After cessation of flow, the optical retardation grows linearly with time until the sample turns turbid (for example,[3] for t_{cryst} up to approximately 100 s, for $T_{cryst} = 141$ °C, $\sigma_w = 0.06$ MPa, $t_s = 12$ s). A linear increase in retardation after intense shearing has also been reported by Liedauer et al.[6] As the growth rate of the crystals is constant,[38] this was interpreted to mean that growth from the central line nucleus must be spokelike (volume of oriented crystals $\sim t$) rather than disklike (volume of oriented crystals $\sim t^2$). Our WAXD data indicate that there is a large difference in crystal growth velocity during flow and after cessation of flow. For the case analyzed in detail in the first part of this paper ($T_{cryst} = 141$ °C, $\sigma_w = 0.06$ MPa, $t_s = 12$), crystallinity develops rapidly during flow, but growth rates slow down to quiescent values after cessation of flow (Figure 5, $x_c \approx 0.03$ after 12 s of flow, $x_c \approx 0.06$ at $t_{cryst} = 150$ s). This gives rise to a pseudolinear increase in the volume of oriented crystals after cessation of flow for disklike growth of the crystals. Further details are given as Supporting Information. The combination of WAXD and birefringence measurements shows that it is not necessary to invoke a $t^{1/2}$ scaling of growth velocity or growth of crystals in the form of radiating spokes from a central cylindrical nucleus. Crystals growing out as disklike

kebabs off the central shish can account for the lineartime dependence due to the difference in growth rates during and after imposition of flow.

5. Conclusions

Synchrotron SAXS and WAXD complement our previous rheooptical,[3,4] optical microscopy,[3] and TEM[4,24] studies on the same isotactic polypropylene sample in "short-term" shearing experiments. Taken together, these results provide a detailed mechanistic picture of the effect of shear on the morphology (crystal anisotropy and orientation distribution, parent:daughter ratio in α-iPP, spatial distribution of crystallites) and kinetics of crystal nucleation and growth. Upon imposition of shear, nucleation is enhanced and crystallization is highly accelerated. The behavior accords qualitatively with the two stages described by Janeschitz−Kriegl with the flow first inducing small, widely spaced precursors, followed later by the formation of threadlike precursors provided that the applied stress is above a threshold value, σ_{crit}, and the flow is imposed for a long enough time. Rather than truly "pointlike" nuclei, the early flow-induced precursors are needlelike, anisotropic crystalline nuclei, aligned with their *c*-axis along the flow direction. For $\sigma_w < \sigma_{crit}$ and for $\sigma_w > \sigma_{crit}$ applied for very short shearing durations (e.g., $t_s = 1$ s at $\sigma_w =$ 0.06 MPa and $T_{cryst} = 141$ °C), the needles formed during shear are not highly extended. As growth proceeds following cessation of flow, noncrystallographic branching causes the lamellae growing off these short needles to splay, resulting in a progressive broadening of the orientation distribution. WAXD azimuthal scans indicate that increasing t_s leads to greater anisotropy, viz. the needlelike nuclei extend during shear. The effect of shear stress (σ_w) is highly nonlinear and is stronger than the effect of t_s, in qualitative accord with the prior literature. Critical value ($\sigma_w > \sigma_{crit}$) flow can generate threadlike precursors that are tens of microns long in a matter of a few seconds. The lamellae that grow out from them are densely nucleated and cannot splay. Thus, the orientation distribution of the threadlike precursors that is established during shear templates the orientation of the crystallites that grow off them, manifested in sharp WAXD peaks that hardly broaden during the time that the cyllindrulites grow to impingement. The row nucleated structure reaches impingement on a time scale that is highly accelerated compared to quiescent crystallization (e.g., merely 1% of the quiescent crystallization time at 141 °C following 12 s shear at $\sigma_w = 0.06$ MPa) due to the short distance between the threadlike precursors.

The lateral growth that occurs during shear at high stress is characterized by a greater growth velocity and a higher ratio of parent:daughter crystallites than the growth that occurs following cessation of flow. Thus, flow preferentially enhances the growth of crystallites that have their *c*-axis along the flow direction. This enhancement of the growth velocity can be quite substantial. For example, the crystallinity index just after cessation of 12 s of shear at $\sigma_w = 0.06$ MPa at 141 °C is already approximately half the value of x_c at impingement. On this basis, the growth velocity of the cyllindrulites during shear is an order of magnitude faster than the quiescent growth velocity.

Acknowledgment. Support for this research was provided by the NSF (DMR-9901403 and DMR-0216491). X-ray experiments were performed at the National Synchrotron Light Source, Brookhaven National Laboratory, which is supported by the Department of Energy, Division of Materials Sciences (DE-AC02-98CH10886 and DE-FG02-99ER45760). We are very grateful to Prof. Buckley Crist for detailed comments on the manuscript.

Supporting Information Available: The Supporting Information describes the calculations of the time-evolution of highly-oriented crystallization for cases in which the growth velocity is much faster during flow than after cessation of flow; it includes a figure that shows a typical time profile illustrating the resulting pseudo-linear growth of cyllindrulites following cessation of shear. This material is available free of charge via the Internet at http://pubs.acs.org.

References and Notes

(1) van Krevelen, D. *Chimia* **1978**, *32*, 279−294.
(2) Kumaraswamy, G.; Verma, R. K.; Kornfield, J. A. *Rev. Sci. Instrum.* **1999**, *70*, 2097−2104.
(3) Kumaraswamy, G.; Issaian, A. M.; Kornfield, J. A. *Macromolecules* **1999**, *32*, 7537−7547.
(4) Kumaraswamy, G.; Verma, R. K.; Issaian, A. M.; Wang, P.; Kornfield, J. A.; Yeh, F.; Hsiao, B. S.; Olley, R. H. *Polymer* **2000**, *41*, 8931−8940.
(5) Kumaraswamy, G.; Kornfield, J. A.; Yeh, F.; Hsiao, B. S. *Macromolecules* **2002**, *35*, 1762−1769.
(6) Liedauer, S.; Eder, G.; Janeschitz-Kriegl, H.; Jerschow, P.; Geymayer, W.; Ingolic, E. *Int. Polym. Proc.* **1993**, *8*, 236−244.
(7) Ulcer, Y.; Cakmak, M. *Polymer* **1997**, *38*, 2907−2923.
(8) Fitchmun, D. R.; Mencik, Z. *J. Polym. Sci., Polym. Phys.* **1973**, *11*, 951−971.
(9) Meijer, H. E. H., Ed.; *Materials Science and Technology*; Wiley-VCH: New York, 1997; Vol. 18.
(10) Choi, K. J.; Spruiell, J. E.; White, J. L. *J. Polym. Sci., Polym. Phys.* **1982**, *20*, 27−47.
(11) Kwack, T. H.; Han, C. D. *J. Appl. Polym. Sci.* **1988**, *35*, 363−389.
(12) Isayev, A. I.; Chan, T. W.; Shimojo, K.; Gmerek, M. *J. Appl. Polym. Sci.* **1995**, *55*, 807−819.
(13) Fujiyama, M.; Wakino, T.; Kawasaki, Y. *J. Appl. Polym. Sci.* **1988**, *35*, 29−49.
(14) Ezquerra, T. A.; Lopez-Cabarcos, E.; Hsiao, B.; Balta-Calleja, F. *Phys. Rev. E* **1996**, *54*, 989−992.
(15) Cakmak, M.; Teitge, A.; Zachmann, H.; White, J. *J. Polym. Sci., Polym. Phys.* **1993**, *31*, 371−381.
(16) Ryan, A.; Patrick, J.; Fairclough, A.; Terrill, N.; Olmstead, P.; Poon, W. *Faraday Discuss.* **1999**, *112*, 13−29.
(17) Pople, J. A.; Mitchell, G. R.; Sutton, S. J.; Vaughan, A. S.; Chai, C. K. *Polymer* **1999**, *40*, 2769−2777.
(18) Somani, R. H.; Hsiao, B. S.; Nogales, A.; Srinivas, S.; Tsou, A. H.; Sics, I.; Balta-Calleja, F. J.; Ezquerra, T. A. *Macromolecules* **2000**, *33*, 9385−9394.
(19) Somani, R. H.; Hsiao, B. S.; Nogales, A.; Fruitwala, H.; Srinivas, S.; Tsou, A. H. *Macromolecules* **2001**, *34*, 5902−5909.
(20) Nogales, A.; Hsiao, B. S.; Somani, R. H.; Srinivas, S.; Tsou, A. H.; Balta-Calleja, F. J.; Ezquerra, T. A. *Polymer* **2001**, *42*, 5247−5256.
(21) Liedauer, S.; Eder, G.; Janeschitz-Kriegl, H. *Int. Polym. Proc.* **1995**, *10*, 243−250.
(22) Jerschow, P.; Janeschitz-Kriegl, H. *Rheol. Acta* **1996**, *35*, 127−133.
(23) Jerschow, P.; Janeschitz-Kriegl, H. *Int. Polym. Proc.* **1997**, *12*, 72−77.
(24) Kornfield, J. A.; Kumaraswamy, G.; Issaian, A. M. *Ind. Eng. Chem. Res.* **2002**, *41*, 6383−6392.
(25) Strobl, G. R.; Schneider, M. *J. Polym. Sci., Polym. Phys.* **1980**, *18*, 1343−1359.
(26) Ruland, W. *Colloid Polym. Sci.* **1977**, *255*, 419−427.
(27) Stribeck, N.; Ruland, W. *J. Appl. Crystallogr.* **1978**, *11*, 535−539.
(28) Santa-Cruz, C.; Stribeck, N.; Zachmann, H. G.; Balta-Calleja, F. J. *Macromolecules* **1991**, *24*, 5980−5990.
(29) Hsiao, B. S.; Verma, R. K. *J. Synchrotron Rad.* **1998**, *5*, 23−29.
(30) Albrecht, T.; Strobl, G. *Macromolecules* **1995**, *28*, 5267−5273.
(31) Ryan, A. J.; Stanford, J. L.; Bras, W.; Nye, T. M. W. *Polymer* **1997**, *38*, 759−768.

(32) Vleeshouwers, S. *Polymer* **1997**, *38*, 3213−3221.
(33) Alexander, L. E. *X-ray Diffraction Methods in Polymer Science*; Wiley-Intescience: New York, 1969.
(34) Baltá-Calleja, F. J.; Vonk, C. G. *X-ray Scattering of Synthetic Polymers*; Elsevier: Amsterdam, 1989.
(35) Formation of interlamellar stacks might decrease the invariant but would also lead to a change in the long spacing. We do not observe a change in long spacing. Therefore, rather than the formation of interlamellar stacks, it is likely that interlamellar densification happens via the formation of small imperfect crystals. Daughter lamellae are epitaxially nucleated on the parents but are not confined within the interlamellar regions (see TEM in Kumaraswamy et al.[4]) These daughter lamellae grow nearly perpendicular to the parents and reduce the electron density difference (spatially averaged over the region of the lamellar stack that gives rise to the SAXS) between the parent lamellae.
(36) Dean, D. M.; Rebenfeld, L.; Register, R. A.; Hsiao, B. S. *J. Mater. Sci.* **1998**, *33*, 4797−4812.
(37) Lotz, B.; Wittmann, J. C.; Lovinger, A. J. *Polymer* **1996**, *22*, 4979−4992.
(38) White, H. M.; Bassett, D. C. *Polymer* **1997**, *38*, 5515−5520.
(39) Padden, F. J., Jr.; Keith, H. D. *J. Appl. Phys.* **1959**, *30*, 1479.
(40) Janimak, J. J.; Cheng, S. Z. D.; Giusti, P. A.; Hsieh, E. T. *Macromolecules* **1991**, *24*, 2253−2260.
(41) For conditions that showed very little orientation, the extremely broad peaks made it difficult to accurately determine the baseline value, and therefore, the data could not be fitted to determine the fwhm of the peaks, the parent-to-daughter ratio or the ratio of oriented to unoriented crystal fraction.
(42) There is a slight distortion in the shape of the daughter peaks since the WAXD pattern is obtained using a flat plate CCD. As the daughter peaks are not located on the meridian (horizontal direction in Figure 9), we expect the contribution from this distortion to be small and neglect it in our calculations.
(43) The ratio of the diffracted crystal intensity from oriented crytals relative to that from an isotropic distribution of the same number of plane normals is given by[36] oriented/isotropic $= 2/[\pi \cos(\theta) \sin(\phi)]$, where θ is the Bragg diffraction angle and ϕ is the angle made by the normal of the crystal plane to the symmetry (flow) direction. On the basis of this equation, we have determined that a *c*-axis-oriented volume of crystals gives a lower diffraction intensity as compared to if the same volume were isotropically distributed.
(44) Vleeshouwers, S.; Meijer, H. *Rheol. Acta* **1996**, *35*, 391−399.
(45) Karger-Kocsis, J., Ed.; *Polypropylene*; Chapman and Hall: London, 1995; Vol. 1.

MA035840N